

# Monte Carlo Simulation on Aging Processes within One ‘Pure State’ of the SK Spin-Glass Model

Hajime Takayama<sup>1</sup>, Hajime Yoshino<sup>2</sup> and Koji Hukushima<sup>3</sup>

Institute for Solid State Physics, University of Tokyo,  
7-22-1 Roppongi, Minato-ku, Tokyo 106, Japan

PACS Number: 02.50.Ey, 75.10.Nr.

submitted to Journal of Physics. A: Mathematical and General

## Abstract

Monte Carlo simulations on the SK model have been done to investigate aging processes after a rapid quench from  $T = \infty$  to the spin-glass phase. The time range of simulations is taken care of so that the system does not surmount free-energy barriers between the pure states which are considered to diverge in the thermodynamic limit. We simulate time evolutions of extensive energy of the system, Parisi’s overlap distribution function, auto-correlation and clones-correlation functions, distribution functions of the two correlations, and magnetization induced by the field applied after a certain waiting time. The data simulated exhibit a rich variety of aging phenomena. Most of them can be interpreted in a unified way, though qualitatively, by the scenario of *growth of quasi-equilibrium domains* which we will introduce in this work. More surprisingly, they suggest strongly that a basin of attraction of one dominant pure state spans almost an entire phase space of the system with a common time-reversal symmetry.

---

<sup>1</sup> takayama@issp.u-tokyo.ac.jp

<sup>2</sup>yhajime@ginnan.issp.u-tokyo.ac.jp

<sup>3</sup>fukusima@ginnan.issp.u-tokyo.ac.jp

# 1 Introduction

Since the first observation by Lundgren et al[1] aging phenomena in spin glasses have been extensively studied[2]. They are expected to reveal nature of the low-temperature spin-glass phase which has not yet been settled in spite of nearly two decades of dispute. One of the key concepts on aging phenomena recently introduced by Bouchaud[3] and incorporated in the analytic theories[4][5] is *weak-ergodicity breaking*. It was originally introduced in the argument on the trap model[3]. In a system exhibiting aging phenomena there exist many metastable states, or 'traps'. Depths of the traps are distributed continuously in such a way that the average time for the system to escape from them by thermal activation process is infinite; or, it takes an infinite time for the system to equilibrate. This picture of weak-ergodicity breaking is represented in terms of the spin auto-correlation function  $C(t, t') \equiv N^{-1} \sum_i S_i(t)S_i(t')$  as follows[3][5]:

$$\frac{\partial C(t, t')}{\partial t} \leq 0, \quad \text{and} \quad \frac{\partial C(t, t')}{\partial t'} \geq 0, \quad (1a)$$

$$\lim_{t \rightarrow \infty} \lim_{t' \rightarrow \infty} C(t, t') = q_c \quad (> 0), \quad (1b)$$

$$\lim_{t \rightarrow \infty} C(t, t') = 0 \quad \text{for a fixed } t' \quad (< \infty), \quad (1c)$$

where  $q_c$  is a certain constant.

Various simulations which reproduce some aspects of the experimentally observed aging phenomena have been already reported[6][7][8][9]. But they are not yet satisfactory to be able to understand the phenomena in a unified way. Since the recent phenomenological and theoretical arguments mentioned above, as well as recent analyses on experiments[10][11], are more or less based on the mean-field picture of spin glasses, we believe it is worth examining aging phenomena in the mean-field spin-glass model more in detail by simulations[12]. In the present work therefore we have performed Monte Carlo (MC) simulation on the SK model[13], whose equilibrium properties are well understood[14]. Its purpose is to obtain various information on its aging phenomena, including those which are related to the above-mentioned key concept.

Aging phenomena we are concerned with are non-equilibrium processes toward equilibrium observed in macroscopic systems in long but finite intervals of time. Since, on the other hand, the present simulations are performed only on finite systems with  $N$  spins, we have to take care of their time range. Suppose the system has a certain relaxation time,  $t_{\text{erg}}(N, T)$ , which may depend also on temperature  $T$ , and whose systematic dependence on  $N$  is known. If  $\lim_{N \rightarrow \infty} t_{\text{erg}}(N, T) = \infty$ , simulations on aging phenomena have to be done in the time range of  $t \lesssim t_{\text{erg}}(N, T)$  in order to be free from the finite-size effect.

According to Parisi's picture[14] on the spin-glass phase of the SK model in equilibrium, there are many pure states which are separated from each other by insurmountable free-energy barriers. More explicitly, it was argued that in systems with large  $N$  there exist two types of the free-energy barriers: one between the pure states with a common time-reversal symmetry, and the other between those with opposite time-reversal symmetries[15][16]. The

characteristic times,  $t_{\text{erg}}^{\text{S}}(N, T)$  and  $t_{\text{erg}}^{\text{L}}(N, T)$ , needed to surmount respectively the former and latter barriers are given by (see Fig. 2 below)

$$\ln t_{\text{erg}}^{\text{S}}(N, T) \propto N^{1/4}, \quad \text{and} \quad \ln t_{\text{erg}}^{\text{L}}(N, T) \propto N^{1/2}. \quad (2)$$

Therefore we have to set at least  $t_{\text{max}} < t_{\text{erg}}^{\text{S}}(N, T)$ , where  $t_{\text{max}}$  is the maximum observation time of simulations. In the present work we call such a limited time interval after a rapid quench *aging range*, and a portion of phase space that the system explores within that interval a ‘*pure state*’.

In the present work we simulate time evolution of various quantities after the quench; extensive energy of the system, Parisi’s overlap distribution function, auto-correlation and clones-correlation functions[12][17][18], and distribution functions of the two correlations. The magnetization induced by the field applied after a waiting time  $t_w$  is also investigated. It has turned out that the data simulated exhibit a rich variety of aging phenomena. They indicate complexity of the rugged free-energy structure within the ‘*pure state*’. It is expected to have many free-energy barriers of finite heights which are surmountable within the aging range introduced above. Most of our simulated results can be interpreted in a unified way, though qualitatively, by the scenario of *growth of quasi-equilibrium domains* which we will introduce and explain in this work. Surprisingly, the results suggest that the basin of attraction of one ‘*pure state*’ spans an almost entire phase space with a common time-reversal symmetry. We call this feature the *dynamic dominant pure-states picture*. On equilibrium properties of the SK model, on the other hand, there is the argument[19] that among many pure states only a few (even one) of them dominate the Gibbs-Boltzmann measure. We call this aspect the *static dominant pure-states picture*. Our simulated data imply that the dynamic dominant pure-states picture describes dynamical (or aging) processes in the phase space whose organization of states gives rise to the static dominant pure-states picture for equilibrium.

In the next section the model and method of our simulations are briefly explained. In section 3 we present the results of simulations which are interpreted by our scenario of growth of quasi-equilibrium domains in section 4. The final section is devoted to the concluding remarks.

## 2 Model and Method

By means of the standard heat-bath method of the MC simulation we have studied the  $\pm J$  SK model with mean zero and variance  $(N - 1)^{-1/2}$ [20]. The system sizes examined are  $N = 32 \sim 2048$ , particularly  $N = 128, 512$  in detail. Mainly analyzed in the present work are aging processes after rapid quenches from  $T = \infty$  to  $T$  below the spin-glass transition temperature  $T_c$  ( $= 1$  in the limit  $N \rightarrow \infty$ ). Simulation of this process is to simply perform a MC run at  $T$  starting from a random spin configuration. Physical quantities are obtained by taking average over such  $M$  independent MC runs for each realizations of  $\{J_{ij}\}$  (sample) and over the  $N_s$  samples. Those at time  $t$  (in unit of 1MC step per spin) in each MC run are evaluated by means of the following short time average,

$$A^{(m)}(t) = \frac{1}{\Delta t + 1} \sum_{t' = t - \Delta t}^t a^{(m)}(t'), \quad (3)$$

where  $a^{(m)}(t')$  is the value of quantity  $A$  at step  $t'$  of  $m$ -th MC run, and  $\Delta t \ll t$  (eg.  $\Delta t = 0$  for  $t < 16$  and 511 for  $t \geq 2^{13}$ ). In the present work we put  $M = 10$  and  $N_s = 40 \sim 2000$  depending on  $N$ .

Most of our simulations are performed in the aging range mentioned in the previous section. Here we further make a comment on this time range in relation to the limiting procedures in eqs.(1b, c). For these equations the limit  $N \rightarrow \infty$  is taken before those of  $t'$  and/or  $t$ . Such limiting procedures cannot be carried out in our simulational study on finite systems. In the present work limiting values of the types of eqs.(1b) and (1c) are extrapolated from the following quantities in systems with finite  $N$ : those simulated in the time range  $t \ll t'$  for the type of eq.(1b) and those in  $t \gg t'$  for that of eq.(1c), both  $t$  and  $t'$  being in the aging range.

Another comment is on a cut-off of the aging range in the shorter side. The time range of simulations should not be too short in order to distinguish aging phenomena peculiar to spin glasses from certain initial transient processes expected to exist in any systems. We denote a time-scale of this short cut-off as  $t_{\text{q.e.}}$ . Its explicit value, as well as that of  $t_{\text{max}}$ , will be discussed below referring to our simulated data.

## 3 Results

### 3.1 Energy and Parisi's overlap distribution

Let us first investigate the time evolution of the energy  $E(t_a)$  after the quench at  $t_a = 0$ . As shown in Fig. 1a, the energy per spin drops rapidly and then gradually saturates to the  $N$ -dependent equilibrium value  $E_{\text{eq}}/N$ . Interesting information is obtained when we look at how the extensive energy  $E(t_a)$  approaches to  $E_{\text{eq}}$ . In Fig. 1b we show  $\Delta E(t_a) \equiv E(t_a) - E_{\text{eq}}$  where  $E_{\text{eq}}$  is approximated by  $E(t_{\text{max}})$ . The time  $t_{\text{erg}}^E(N, T)$ , defined by  $\Delta E(t_{\text{erg}}^E) \cong T$ , is shown in Fig. 2. It has the same  $N$ -dependence as that of  $t_{\text{erg}}^S(N, T)$  of eq.(2) obtained previously[15], though the proportional constants are different. In the present work we adopt  $t_{\text{erg}}^E(N, T)$  as the upper boundary of the aging range.

A typical barrier energy  $E_B(t)$  for the system to be able to surmount within time  $t$  is given by  $E_B(t) \simeq T \ln t$ , where the attempt time of thermal activation process is put 1 MC step. The value  $\Delta E(t_a) + E_B(t_a)$  for  $N = 512$  is also shown in Fig. 1b. The data shown in the figure tell that relaxational processes in the aging range are associated with decrease of  $\Delta E(t_a)$  (even of  $\Delta E(t_a) + E_B(t_a)$ ).

In Fig. 3 the time evolution of Parisi's overlap distribution functions  $P(q; t_a)$  is demonstrated for systems with  $N = 128$  at  $T = 0.4$ . Here  $q$  is one of  $M(M-1)/2$  overlaps of magnetization configurations  $q(t) = N^{-1} \sum_i m_i^{(k)}(t) m_i^{(l)}(t)$  where  $m_i^{(k)}(t)$  is evaluated by eq.(3) with  $a = S_i$ . In the figure the thick broken line represents  $P_{\text{RSB}}(q)$ , i.e.,  $P(q)$  in equilibrium and in the thermodynamic limit which is evaluated by solving numerically Parisi's equation[21]. The position of its delta peaks are specified  $\pm q_{\text{EA}}$ ; the self-overlap parameter[14]. As already reported by Bhatt and Young[16],  $P(q; t_a)$  evolves from a single gaussian centered at  $q = 0$  at  $t_a = 0$  to a structure with double peaks (but of significant widths) similar to  $P_{\text{RSB}}(q)$  at large enough  $t_a$ . In the present analysis we determine  $t_{\text{erg}}^L(N, T)$  as the time at which  $P(q \simeq 0; t_a)$  converges to  $P_{\text{RSB}}(q \simeq 0)$  and show it also in Fig. 2. We see in Fig. 3 that at  $t_a = 512 \simeq t_{\text{erg}}^E(N = 128, T = 0.4)$ ,  $P(q; t_a)$  exhibits already the double peaks around

$q = \pm q_{\text{EA}}$  but its peak at  $q \simeq 0$  still remains.

### 3.2 Auto-correlation function

In Fig. 4a we show typical data of the auto-correlation function  $C(t + t_w, t_w)$ . It is obtained at  $T = 0.4$  of systems with  $N = 512$  in the aging range, i.e.,  $t_a = t + t_w \lesssim t_{\text{erg}}^E(N = 512, T = 0.4) \simeq 3 \times 10^4$ . One can see that  $C(t + t_w, t_w)$  satisfies eq.(1a), i.e., one of the conditions of the weak-ergodicity breaking. Also the data exhibit crossover behavior from relatively slow decay in  $t < t_w$  to relatively rapid decay in  $t > t_w$ . The behavior is common to  $C(t + t_w, t_w)$  simulated in various systems[6][7][8][22], and is interpreted as a crossover from quasi-equilibrium to out-of-equilibrium behaviors.

An interesting feature becomes clear if we plot  $C(t + t_w, t_w)$  against  $\ln(t/t_w)$ , as shown in Fig. 4b. As first pointed out by Baldassarri[12],  $C(t + t_w, t_w)$  with different  $t_w$  cross almost at a point  $t \simeq t_{\text{crs}}$ . This behavior is certainly different from those of  $C(t + t_w, t_w)$  observed in the previous works[7][8][22], whose  $C(t + t_w, t_w)$  with different  $t_w$ 's in the out-of-equilibrium range are well scaled to a single curve when plotted against  $t/t_w$ . We also note that  $\ln t_{\text{crs}} \simeq \ln t_w$  and that the value of  $C(t_{\text{crs}} + t_w, t_w)$  is rather closer to  $1 - T = \bar{q}$  than  $q_{\text{EA}}$  ( $\simeq 0.75$ ), where  $\bar{q} = \int_0^1 q(x)dx$  is Parisi's order parameter in equilibrium[14].

That the above crossing feature of  $C(t + t_w, t_w)$  is a genuine property of aging processes in the present system is ascertained by the inspection of  $C(t_a, t_a/2)$  which can be simulated by single aging process. As shown in Fig. 5  $C(t_a, t_a/2)$  for various  $N$  and  $T$  are nearly independent of  $t_a$  in the range  $t_1 \lesssim t_a \lesssim t_2(N, T)$ . Here  $t_2(N, T)$  is a time around which  $C(t_a, t_a/2)$  starts to decrease from its nearly constant value, and we have checked that it coincides with  $t_{\text{erg}}^E(N, T)$  within logarithmic accuracy. On the other hand, the shorter time scale  $t_1$  is regarded as  $t_{\text{q.e.}}$  mentioned in section 2. The near constancy of  $C(t_a, t_a/2)$  implies that  $C(t + t_w, t_w)$  with different  $t_w$ 's have a nearly common value at  $\ln(t/t_w) \simeq 0$ .

### 3.3 Clones-correlation function

We have also investigated the clones-correlation function  $Q(t + t_w, t_w)$  [12][17][18]. It is the correlation of two configurations starting from an identical one which has evolved up to  $t_a = t_w$ , but are evolving by means of two independent MC runs (with different sets of random numbers) at  $t_a > t_w$ . A typical result is shown in Fig. 6 for  $T = 0.4, N = 512$ . As found also by Baldassarri[12],  $C(t + t_w, t_w)$  and  $Q(t + t_w, t_w)$  cross at  $\ln t \sim \ln t_w$ . Their values at the crossing are again closer to  $\bar{q}$  independently of  $t_w$ . A more remarkable feature seen in the figure is that  $Q(t + t_w, t_w)$  with fixed  $t_w$  tend to saturate to constant values which depend on  $t_w$  as  $t \rightarrow t_{\text{erg}}^E(N, T)$ . It is also noted (not shown) that  $Q(t + t_w, t_w)$  plotted against  $\ln(t/t_w)$  also cross nearly at a point similarly to  $C(t + t_w, t_w)$  in Fig. 4b.

### 3.4 Fluctuation-dissipation theorem

In order to get further insights into aging processes we have simulated the magnetization  $m(t; t_w)$  induced by the field  $h$  which is switched on at  $t_a = t_w$ . The result for  $T = 0.4, N = 512$  and with  $h = 0.1$  is drawn against  $\ln(t/t_w)$  in Fig. 7. Also shown by broken lines in the figure are  $m_C(t; t_w)$  defined by

$$m_C(t; t_w) = h\{1 - C(t + t_w, t_w)\}/T. \quad (4)$$

The fluctuation-dissipation theorem (FDT) tells that, in equilibrium and for an infinitesimally small  $h$ ,  $m(t; t_w)$  and  $m_C(t; t_w)$  are independent of  $t_w$  and  $m(t) = m_C(t)$  holds. We see in Fig. 7 that, as has been also observed in other model systems[6][9][22],  $m(t; t_w) \cong m_C(t; t_w)$  holds in the time range  $t \ll t_w$  with  $t_w$  larger than a certain value. The latter value, which roughly coincides with  $t_1$  introduced above, is also used to estimate  $t_{\text{q.e.}}$  which specifies the initial transient regime of the aging process.

## 4 Discussions

### 4.1 Scenario of growth of quasi-equilibrium domains

In order to interpret the above results of our simulations, let us first remind of the following properties of the SK model in equilibrium. It is known that the TAP equation[24] of the SK model has a huge number of solutions, or local free-energy minima, in the spin-glass phase[25]. In equilibrium, however, only a very limited number of the local minima have significant probability weights  $P_\alpha (\propto \exp(-F_\alpha/T))$  where  $F_\alpha$  is the (extensive) TAP free-energy of the  $\alpha$ -th solution[19] (the *static dominant pure-states picture* mentioned in §1). Associated with such lowest free-energy states are limited portions of phase space which are separated by free-energy barriers described by eq.(2). One of the possible interpretations is then that aging processes simulated in the present work reflect the free-energy structures of such local regions centered at each lowest free-energy state. We may identify these regions to the ‘pure states’ introduced in section 1.

Based on the above assumption we argue that each ‘pure state’ contains a huge number of local minima (which we call hereafter simply states), as schematically shown in Fig. 8. The lower their (extensive) energies, the less is the number of the states. [Here and hereafter we disregard entropy effects which have not been evaluated explicitly in the present simulation.] Their basins of attraction for a rapid quench process are considered to have more or less comparable sizes[26]. Therefore after a certain initial transient time the system is found, with probability of almost unity, in one of the huge number of states with a relatively higher energy, from which it starts to look for lower and lower energy states by thermal activation processes; i.e., it ages. We consider that  $t_{\text{q.e.}}$  introduced before corresponds to the above-mentioned transient time. It is noted that  $t_{\text{q.e.}}$  are little dependent on  $N$  and is less than a few tens MC steps (see Figs. 5 and 7).

Let us then suppose that at time  $t_a = t_{w1}$  in the aging range the system reaches to a certain state, say  $S_1$  in Fig. 8. In a time interval of  $t_a = t_{w1} + t$  with  $t \ll t_{w1}$  the system is fluctuating in a local region  $R_1$  centered at  $S_1$  (the shaded area in Fig. 8), thereby it is expected to visit states in the region with frequencies according to their relative Boltzmann weights. We call such regions *quasi-equilibrium domains*. As time goes on another interval of order  $t_{w1}$ , i.e., at  $t_a = t_{w2} \simeq 2t_{w1}$ , the system surmounts a barrier of order  $T \ln t_{w1}$  and finds a lower energy state, say  $S_2$  in Fig. 8. This corresponds to entering into the out-of-equilibrium range of the waiting time  $t_{w1}$ . The state  $S_2$  is, in turn, associated with the quasi-equilibrium domain  $R_2$  of the waiting time  $t_{w2}$  which is larger than  $R_1$ . The quasi-equilibrium domain grows with time until it exhausts the whole ‘pure state’, or the system reaches the lowest energy state  $S_\infty$  in Fig. 8 (which takes an infinite time if  $N = \infty$ ).

The above scenario for aging processes, which we call *growth of quasi-equilibrium domains*,

has been initially introduced from our relaxational-modes analysis on the same problem[27]. From the present MC study it is introduced to explain straightforwardly the following results in the aging range of  $t_{\text{q.e.}} \lesssim t_a \lesssim t_{\text{erg}}^E(N, T)$ : 1) the monotonic decrease of the extensive energy in the aging range ( $\Delta E(t_a)$  in Fig. 1b), 2) the crossover from quasi-equilibrium to out-of-equilibrium behaviors at around  $t \sim t_w$  seen in  $C(t + t_w, t_w)$  of Fig. 4, 3) the apparent FDT at  $t \ll t_w$  demonstrated in Fig. 7, and 4) the behavior of the clones-correlation shown in Fig. 6 which is explained as follows. Suppose the clones are created at  $t_a = t_{w1}$  from a spin configuration near  $S_1$  in Fig. 8. Then at  $t \gtrsim t_{w1}$ , the clones visit more frequently near the same state  $S_2$  whose relative Boltzmann weight is largest in the larger domain  $R_2$ . The Hamming distance between them is then considered to be smaller than that between  $S_1$  and  $S_2$  which determines predominately the value of the corresponding auto-correlation function. This means  $Q(t + t_{w1}, t_{w1}) > C(t + t_{w1}, t_{w1})$  at  $t \gtrsim t_{w1}$  as observed in the simulation.

Concerned with the above items 2) and 3), we note that at  $t \ll t_w$   $C(t + t_w, t_w)$  depend not only on  $t$  but also on  $t_w$  (see Fig. 4a). This means that nature of overall fluctuation within each quasi-equilibrium domain differs between the domains and from true equilibrium. Still  $C(t + t_w, t_w)$  and  $m(t; t_w)$  obey the apparent FDT. This feature is certainly different from the recent arguments[5][10] that both  $C(t + t_w, t_w)$  and  $m(t; t_w)$  consist of two parts, equilibrium and aging ones, and that the FDT holds only for the equilibrium parts which depend on  $t$  alone.

We also note that the above time range  $t_w \gg t$  ( $\gtrsim t_{\text{q.e.}}$ ) is the one where we look for the limiting value of eq.(1b) as pointed out in Section 2. Naive speculation based on the results shown in Figs. 4b and 5 is that  $q_c$  in eq.(1b) is certainly less than  $q_{\text{EA}}$  in contrast to the previous claim of  $q_c = q_{\text{EA}}$ [5]. In our simulation on a large but finite  $N$  system, we regard that the system is in ‘equilibrium’ within one ‘pure state’ at  $t_w$  of the order of  $t_{\text{erg}}^E(N, T)$ . The extrapolation to  $N = \infty$  keeping these conditions at  $t_w \sim t_{\text{erg}}^E(N, T)$  gives rise to  $q_c$  smaller than  $q_{\text{EA}}$ .

## 4.2 Distribution functions of clone- and auto-correlations

The time evolution of distribution functions  $P(Q; t, t_w)$  with  $Q(t) = N^{-1} \sum_i m_i^{[1]}(t) m_i^{[2]}(t)$  shown in Fig. 9a further supports the above interpretation of the clones-correlation. Here  $m_i^{[k]}(t)$  is evaluated by eq.(3) whose  $a$  in the r.h.s. is  $S_i$  of the  $k$ -th clone. The distribution is therefore obtained from  $MN_s$  data points of  $Q(t)$ . A sharp peak of  $P(Q; t, t_w)$  at  $t \ll t_w$  located around  $Q \simeq q_{\text{EA}}$  indicates simply that the clones are not yet separated enough and are fluctuating near the lowest energy state in the quasi-equilibrium domain of waiting time  $t_w$ . Around  $t \simeq t_w$  height of the peak decreases and its width increases. This is interpreted that the clones now tend to escape statistically independently of each other from the domain of  $t_w$ . Interestingly at  $t \gg t_w$  the peak near  $Q \simeq q_{\text{EA}}$  sharpens again though its height does not recover very much. The peak in this time range suggests that the clones are again near the same lowest energy state but of a larger quasi-equilibrium domain than the original one. This implies that  $Q(t + t_w, t_w)$  for fixed  $t_w$  converge to certain finite values. This is in fact the case as we have already seen in Fig. 6;  $Q(t + t_w, t_w)$  almost saturate to certain constants. Correspondingly, the shape of  $P(Q; t, t_w)$  becomes little dependent on  $t$  at  $t$  ( $\sim t_{\text{erg}}^E(N, T)$ ).

In order to examine the  $N$ -dependence of the above characteristic feature in the clones-correlation, we show in Fig. 9b  $Q(t + t_w, t_w)$  at  $t \simeq t_{\text{erg}}^E(N, T)$  for  $N = 128$  and  $512$  both with

$t_w=64$ . The two almost coincide with each other. The small difference in the peak positions near  $Q = q_{EA}$  is attributed to the finite-size effect. Naive extrapolation of these results to  $N \rightarrow \infty$  (thereby  $t_{\text{erg}}^E(N, T) \rightarrow \infty$ ) is  $\lim_{t \rightarrow \infty} Q(t + t_w, t_w) > 0$  for a fixed  $t_w (< \infty)$ . Thus the aging process within one ‘pure state’ of present interest belongs to type I by means of the classification introduced by Barrat et al[18].

In Fig. 9b we also show, by the thin solid curve,  $Q(t + t_w, t_w)$  at  $t \simeq t_{\text{erg}}^L(N, T)$  for  $N = 128$ . One sees that a small peak starts to develop not around  $Q = 0$  but around  $Q = -q_{EA}$ . This result is interpreted as follow. When one of the clones surmounts the energy barrier between the phase spaces with different time-reversal symmetry, it goes down and situates near the counterpart of  $S_\infty$  within a time interval of  $t_{\text{erg}}^E(N, T) (\ll t_{\text{erg}}^L(N, T))$ .

In contrast to  $Q(t + t_w, t_w)$  above discussed,  $C(t + t_w, t_w)$  in Fig. 6 doesn’t exhibit tendency of the saturation to certain finite values within the aging range of the present concern. Although it neither completely vanishes in the same time range, we expect that the weak-ergodicity breaking condition of eq.(1c) holds in the limit  $N \rightarrow \infty$  within its aging range. This expectation is derived from inspection of the distribution functions of auto-correlation,  $P(C; t, t_w)$  with  $C(t) = N^{-1} \sum_i S_i(t + t_w) S_i(t_w)$ , shown in Fig. 10. At  $t > t_w$ , in contrast to  $P(Q; t, t_w)$ ,  $P(C; t, t_w)$  tends to become a gaussian form whose center tends to approach  $C = 0$ . We therefore consider that the weak-ergodicity breaking of eq.(1c) holds since any configuration at  $t_a = t_w (< \infty)$  in a ‘pure state’ is orthogonal to (separated far away from) the configuration at  $t_a = \infty$ , i.e., the lowest energy state of the ‘pure state’.

According to Barrat et al[18], the above aging process of type I judging from  $Q(t + t_w, t_w)$  and with the weak-ergodicity breaking judging from  $C(t + t_w, t_w)$ , is expected to appear, for example, in a system having a ‘gutter’ in phase space. But our scenario of growth of quasi-equilibrium domains is also compatible with the two characteristics. We only need a quite natural assumption that a basin of attraction of a ‘pure state’ is infinitely large if  $N = \infty$ . In fact our scenario is more appropriate judging from the time evolution of  $P(Q; t, t_w)$  already described above. We may say that the energy structure in one ‘pure state’ is, instead of a ‘gutter’, a ‘funnel’ with an infinitely wide input-mouth.

### 4.3 Dominant pure-states pictures

Lastly let us compare the three distribution functions  $P(Q; t \sim t_{\text{erg}}^E, t_w)$ ,  $P(q; t_a \simeq t_{\text{erg}}^E)$  and  $P_{\text{RSB}}(q)$  drawn in Fig. 9c. Here  $P(q; t_a \simeq t_{\text{erg}}^E)$  and  $P_{\text{RSB}}(q)$  (also those in Figs. 9a,b) are normalized as  $\int_{-1}^1 P(q) dq = 2$ , differently from those in Fig. 3. The reason of this normalization is that time evolution of the clones at  $t \sim t_{\text{erg}}^E(N, T) (\ll t_{\text{erg}}^L(N, T))$  of present interest is almost confined in a part of phase space with a common time-reversal symmetry. [A small weight of  $P(Q; t, t_w)$  smearing out to  $Q < 0$  is considered due to the finite-size effect]. It is rather surprising that near coincidence,  $P(Q; t \sim t_{\text{erg}}^E, t_w) \simeq P(q; t_a \simeq t_{\text{erg}}^E(N, T)) \simeq P_{\text{RSB}}(q)$ , holds for  $Q, q \gtrsim 0.3$ . [To be more accurate, near equality  $P(q; t_a) \cong P_{\text{RSB}}(q)$  for all  $q$  is obtained only at  $t$  larger than  $t_{\text{erg}}^L(N, T)$  as seen in Fig. 3 and in the previous work[16]. By ‘near coincidence’ here we disregard quantitative difference in the weights associated with the peak at  $Q, q \simeq q_{EA}$  and qualitative difference in the shapes at  $Q, q \lesssim 0.3$ .]

The near coincidence  $P(Q; t \sim t_{\text{erg}}^E, t_w) \simeq P_{\text{RSB}}(q)$  alone indicates that the organization of states in one ‘pure state’ centered at the lowest energy state ( $S_\infty$  in Fig. 8) is similar to that of the whole phase space with a common time-reversal symmetry which gives rise to

$P_{\text{RSB}}(q)$ . The other near coincidence  $P(Q; t \sim t_{\text{erg}}^{\text{E}}, t_w) \simeq P(q; t_a \simeq t_{\text{erg}}^{\text{E}})$  tells more since its r.h.s. quantity is the overlap between two configurations which start from random initial configurations independently chosen. Its plausible interpretation we can think of is that a basin of attraction of one ‘pure state’ reached by our simulation in fact covers almost an entire phase space with a common time-reversal symmetry. This is what we have called the dynamic dominant pure-states picture in section 1. We regard the near coincidence of the three distribution functions as an evidence that the aging processes we have simulated are stochastic dynamics of the system in the phase space, whose organization of states in equilibrium is described by the static dominant pure-states picture[19]. In other words, our present simulations yield, for the first time to our knowledge, an evidence for the latter picture from a dynamical point of view.

## 5 Conclusion

We have proposed the scenario that aging processes at a fixed  $T$  (and  $h$ ) in the SK model, which are observed in the aging range of  $t_{\text{q.e.}} \lesssim t \lesssim t_{\text{erg}}^{\text{E}}(N, T)$ , are growth processes of quasi-equilibrium domains, or stochastic dynamics of the system looking for dominant pure states which exhaust the probability weights in equilibrium. It qualitatively explains most of our simulated results. In our arguments extensive energies of states (solutions of the TAP equation), which are represented by the ordinate of Fig. 8, and which govern relative Boltzmann weights in each quasi-equilibrium domain, play a central role. If, however, we want to know more details of aging phenomena, such as an explicit functional form of  $C(t + t_w, t_w)$ , we have to analyze the organization of the states in the direction of the abscissa of Fig. 8. For this purpose the difference in the extensive energies may not be so important than the above argument (imagine that in the SK model with  $N \rightarrow \infty$  the system is somewhere in the middle of the ‘funnel’ of Fig. 8 at a finite time). The research in this direction is now going on.

Acknowledgements: We are specially indebted to R. Orbach and Y.G. Joh since this work was initiated from discussions with them on their experimental findings. We are grateful to J.-P. Bouchaud, L.F. Cugliandolo and J. Kurchan for many stimulating discussions. We also acknowledge useful discussions with J. Hammann, K. Nemoto, P. Nordblad, M. Ocio, E. Vincent and A.P. Young. The computation in this work has been done using FACOM VPP500 of the Supercomputer Center, Institute for Solid State Physics, University of Tokyo. One of the authors (HY) was supported by Fellowships of the Japan Society for the Promotion of Science for Japanese Junior Scientists. This work is supported by a Grant-in-Aid for International Scientific Research, “Aging Phenomena in Complex Systems” (#08044060), and by a Grant-in-Aid for Scientific Research (#08640477), both from the Ministry of Education, Science and Culture, Japan

## References

- [1] L. Lundgren, P. Svedlindh, P. Nordblad and O. Beckman: Phys. Rev. Lett. **51** (1983) 911.
- [2] E. Vincent, J. Hammann and M. Ocio: in *“Recent Progress in Random Magnets”*, ed. D.H. Ryan (World Scientific, Singapore, 1992), and references therein.
- [3] J.-P. Bouchaud: J. Phys. I France **2** (1992) 1705.
- [4] L.F. Cugliandolo and J. Kurchan: Phys. Rev. Lett. **71** (1993) 173.
- [5] L.F. Cugliandolo and J. Kurchan: J. Phys. A: Math. Gen. **27** (1994) 5749.
- [6] J.-O. Andersson, J. Mattsson and P. Svedlindh: Phys. Rev. B **46** (1992) 8297, **49** (1994) 1120.
- [7] L.F. Cugliandolo, J. Kurchan and F. Ritort: Phys. Rev. B **49** (1994) 6331.
- [8] H. Rieger: in *“Annual Review of Computational Physics”*, vol.II, ed. D. Stauffer, (World Scientific, Singapore, 1995).
- [9] S. Franz and H. Rieger: J. Stat. Phys. **79** (1995) 749.
- [10] E. Vincent, J. Hammann, M. Ocio, J.-P. Bouchaud and L.F. Cugliandolo: preprint cond-mat/9607224.
- [11] Y.G. Joh, R. Orbach and J. Hammann: preprint.
- [12] A. Baldassarri: preprint, cond-mat/9607162.
- [13] D. Sherrington and S. Kirkpatrick: Phys. Rev. Lett. **35** (1975) 1792.
- [14] M. Mézard, G. Parisi and M.A. Virasoro: *“Spin Glass Theory and Beyond”* (World Scientific, Singapore, 1986).
- [15] N.D. Mackenzie and A.P. Young: Phys. Rev. Lett. **49** (1982) 301.
- [16] R.N. Bhatt and A.P. Young: J. Phys. C: Solid State Phys. **21** (1988) L57.
- [17] L.F. Cugliandolo and D.S. Dean: J. Phys. A: Math. Gen. **28** (1995) 4213.
- [18] A. Barrat, R. Burioni and M. Mézard: J. Phys. A: Math. Gen. **29** (1996) 1311.
- [19] M. Mézard, G. Parisi, N. Sourlas, G. Toulouse and M. Virasoro: J. Physique **45** (1984) 843.
- [20] M. Picco and F. Ritort: J. Phys. I France **4** (1994) 1619.
- [21] K. Nemoto: J. Phys. C: Solid State Phys. **20** (1987) 1325.

- [22] H. Yoshino: *J. Phys. A: Math. Gen.* **29** (1996) 1421.
- [23] S. Franz and H. Rieger: *J. Stat. Phys.* **79** (1995) 749.
- [24] D.J. Thouless, P.W. Anderson and R. Palmer: *Phil. Mag.* **35** (1977) 593.
- [25] A.J. Bray and M.A. Moore: *J. Phys. C: Solid State Phys.* **13** (1980) L469.
- [26] K. Nishimura, K. Nemoto and H. Takayama: *J. Phys. A: Math. Gen.* **23** (1990) 5915.
- [27] H. Yoshino, K. Hukushima and H. Takayama: *Prog. Theor. Phys.* to appear (cond-mat/9611230).

## Figure Captions

Fig.1: Time evolution of energy at  $T = 0.4$ . a) Energy per spin in systems with  $N(N_s) = 32(2000)$ ,  $64(2000)$ ,  $96(2000)$ ,  $128(1000)$ ,  $192(600)$ ,  $256(500)$ ,  $512(200)$ ,  $1024(40)$ , and  $2048(50)$  from top to bottom. b) Extensive energy relative to  $E_{\text{eq}}$  for  $N = 32 \sim 512$ . The data with broken line represents  $\Delta E(t_a) + E_B(t_a)$  for  $N = 512$  (see text for definition of  $E_B$ ).

Fig.2: The system-size ( $N$ ) dependence of characteristic relaxation times related to aging processes in the SK model at  $T = 0.4$  for  $N \leq 256$ ;  $t_{\text{erg}}^L(N, T)$  and  $t_{\text{erg}}^S(N, T)$  of eq.(2) and  $t_{\text{erg}}^E(N, T)$  determined by  $\Delta E(t_{\text{erg}}^E) = 0.5$  ( $= 1.2T$ ) from Fig. 2b. The solid line is  $\ln(t_{\text{erg}}^S(N, T)) = 2.56N^{1/4} - 0.66$  due to Ref.[15]. The area below  $t_{\text{erg}}^E(N, T)$  is the aging range introduced and studied in the present work.

Fig.3: Parisi's overlap distribution function  $P(q; t_a)$  for  $N = 128$ ,  $T = 0.4$ . It is normalized as  $\int_{-1}^1 P(q; t) dq = 1$ . The data are  $t_a = 16, 64, 512, 4096$  and  $32768$  from top to bottom at around  $q \simeq 0$ . The thick broken line represents  $P_{\text{RSB}}(q)$ .

Fig.4: Auto-correlation functions  $C(t + t_w, t_w)$  with  $t_w = 2^n$  ( $n = 3 \sim 13$ ) plotted against  $t$  (a) and  $t/t_w$  (b) ( $T = 0.4$ ,  $N = 512$ ,  $N_s = 200$ ).

Fig.5: Auto-correlation functions  $C(t_a, t_a/2)$  for some  $T$  and  $N$ .

Fig.6: Clones-correlation functions  $Q(t + t_w, t_w)$  with  $t_w = 8, 16, 64, 256$  and  $1024$  ( $T = 0.4$ ,  $N = 512$ ,  $N_s = 100$ ). Auto-correlation functions  $C(t + t_w, t_w)$  are also shown by lines with the open symbols. The arrow indicates  $t = t_{\text{erg}}^E(N, T)$ .

Fig.7: Induced magnetization  $m(t; t_w)$  (symbols with solid lines) and  $m_C(t; t_w)$  (broken lines) of eq.(4) with  $t_w = 2^n$  ( $n = 3 \sim 13$ ) plotted against  $t/t_w$  ( $T = 0.4$ ,  $h = 0.1$ ,  $N = 512$ ,  $N_s = 200$ ).

Fig.8: Schematic representation of the rugged energy structure of one 'pure state' of the SK model. The dots represent local energy minima ( $S_1, S_2, \dots, S_\infty$ ) and the shaded areas quasi-equilibrium domains ( $R_1, R_2, \dots$ ).

Fig.9: a) Distribution functions of clones-correlation  $P(Q; t, t_w)$  corresponding to the curve with  $t_w = 64$  in Fig. 6. The broken curve without symbols represents  $P_{\text{RSB}}(q)$  (also in Figs. 9b,c, and 10) b) Comparison of  $P(Q; t, t_w)$  with  $N = 128, 512$  and  $t_w = 64$ : the solid curve with circles represents  $P(Q; t = 512 \simeq t_{\text{erg}}^E, t_w)$  of  $N = 128$ , the broken curve with triangles  $P(Q; t = 2^{15} \simeq t_{\text{erg}}^E, t_w)$  of  $N = 512$ , and the thin solid curve  $P(Q; t = 2^{15} \simeq t_{\text{erg}}^L, t_w)$  of  $N = 128$ . c) Comparison of  $P(Q; t \sim t_{\text{erg}}^E, t_w)$  (broken curve with squares),  $P(q; t_a \simeq t_{\text{erg}}^E)$  (solid curve), and  $\simeq P_{\text{RSB}}(q)$  for  $N = 512$  and  $T = 0.4$ . In this figure  $P(q)$  are normalized as  $\int_{-1}^1 P(q) dq = 2$ .

Fig.10: Distribution functions of auto-correlation  $P(C; t, t_w)$  corresponding to the curve with  $t_w = 64$  in Fig. 6.

## FIGURES

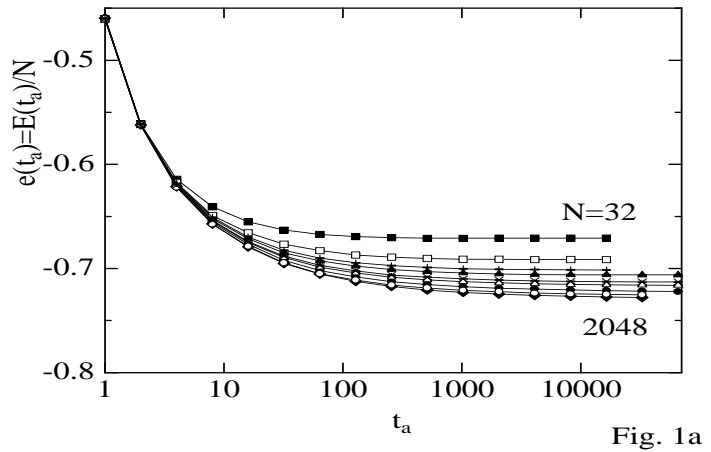


Fig. 1a

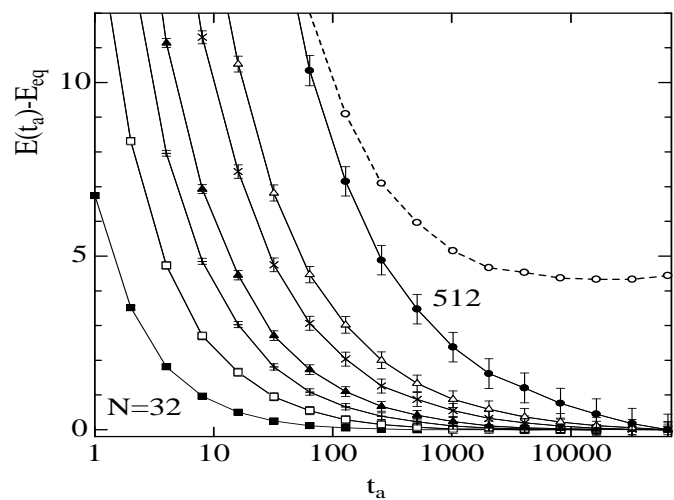


Fig. 1b

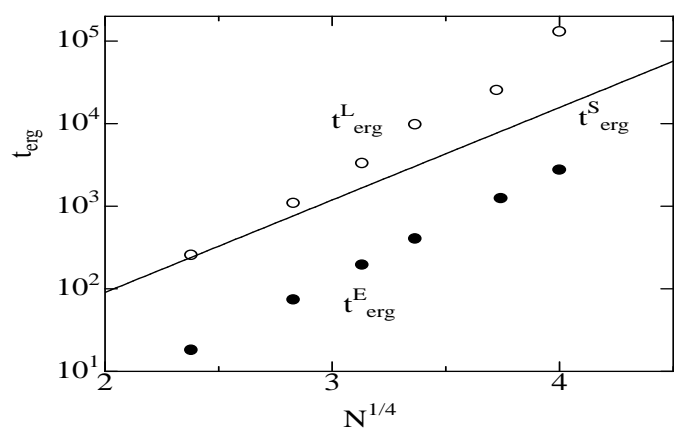


Fig. 2

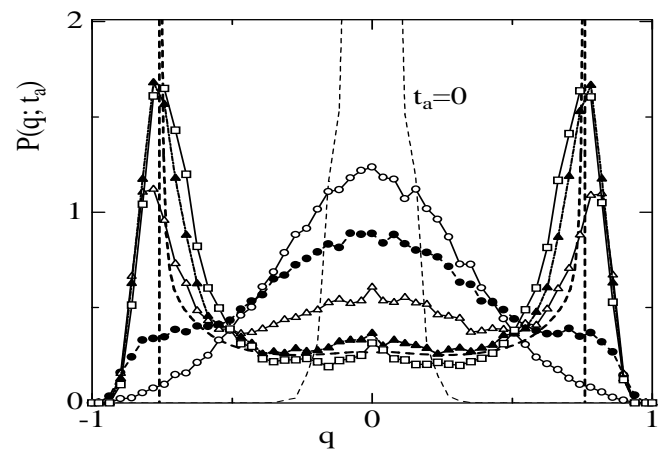


Fig. 3

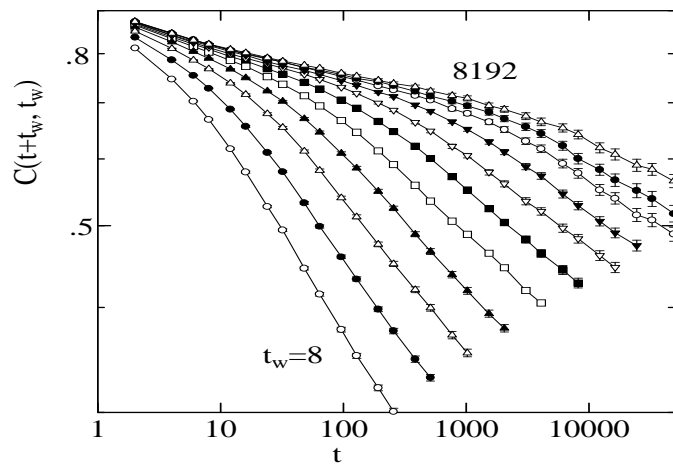


Fig. 4a

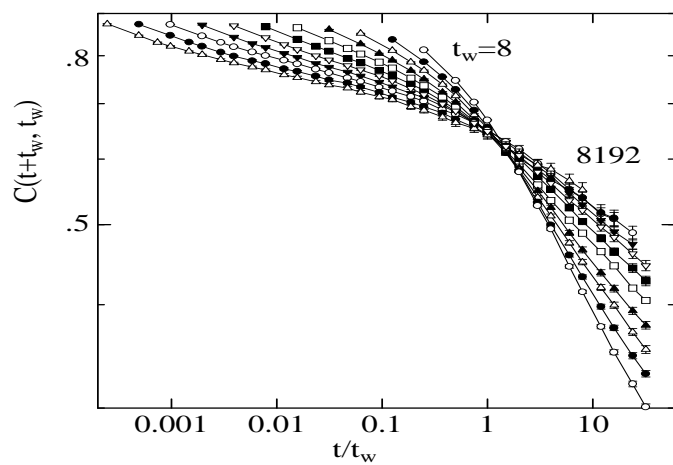


Fig. 4b

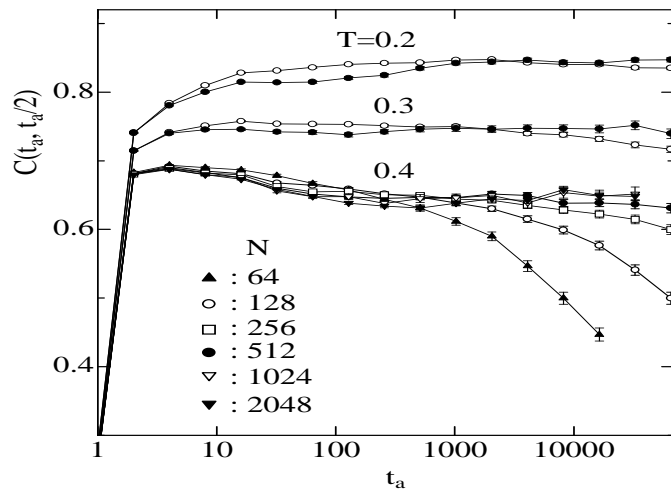


Fig. 5

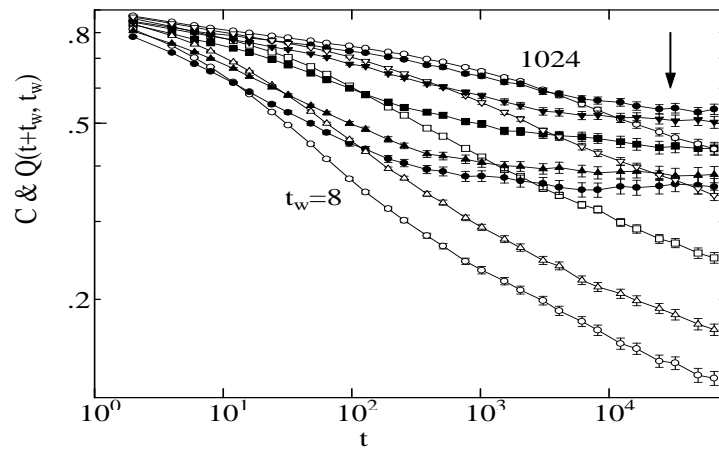


Fig. 6

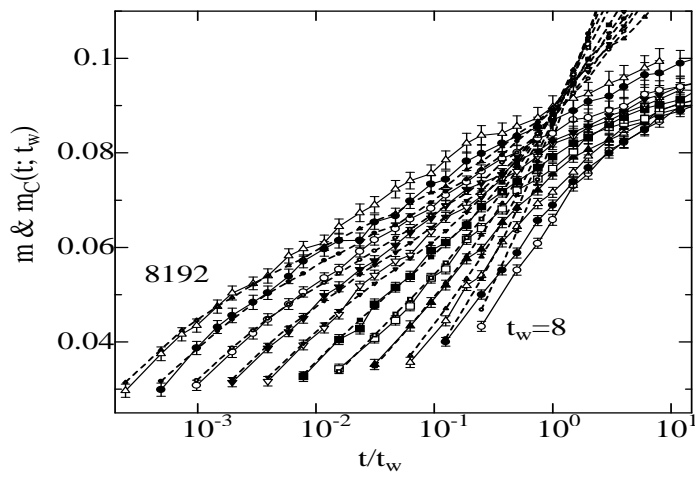


Fig. 7

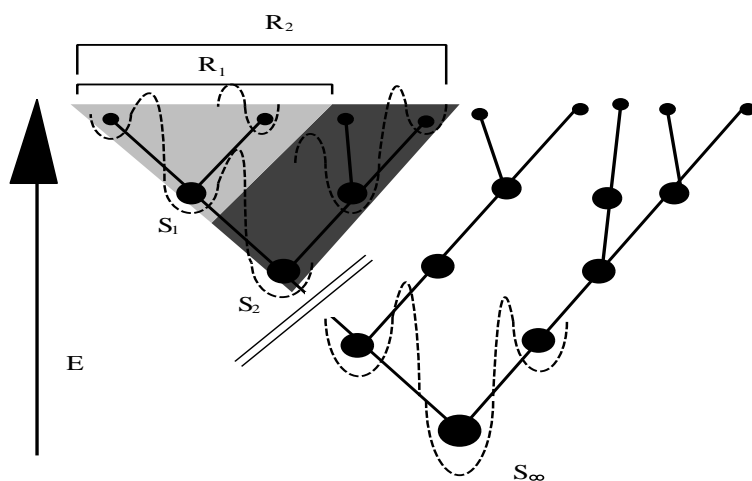


Fig. 8

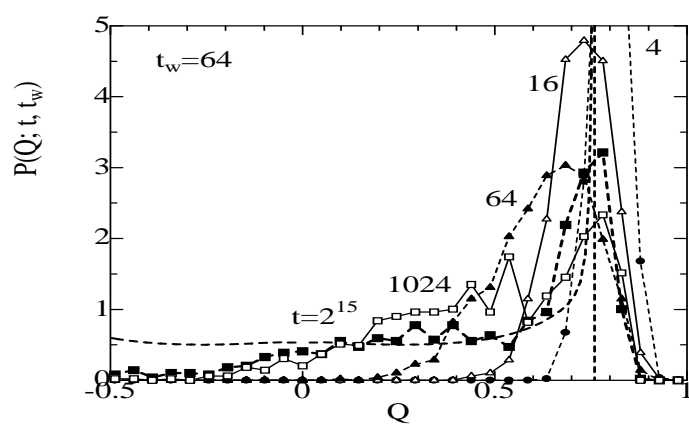


Fig. 9a

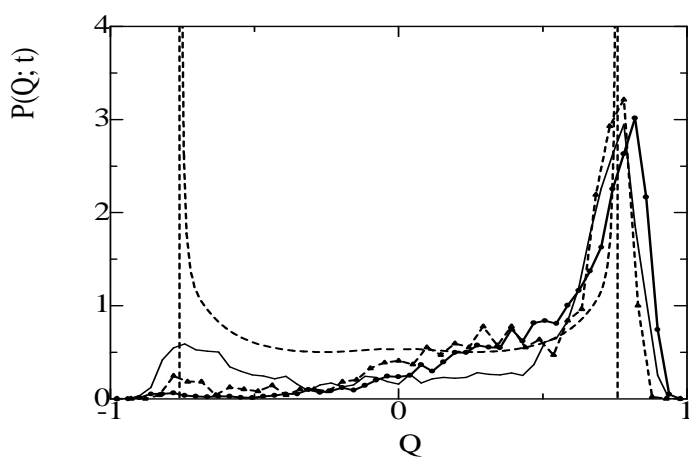


Fig. 9b

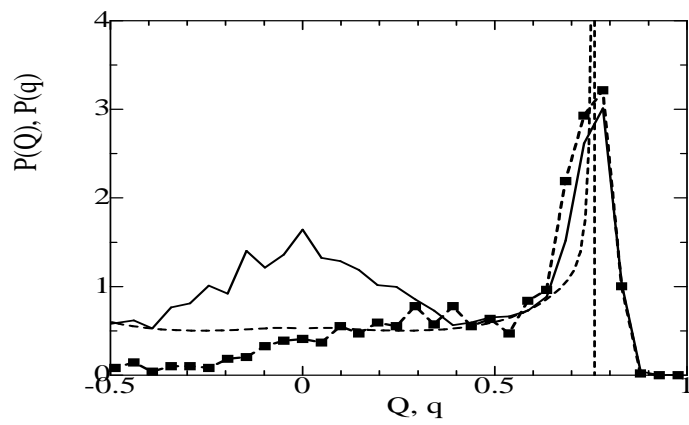


Fig. 9c

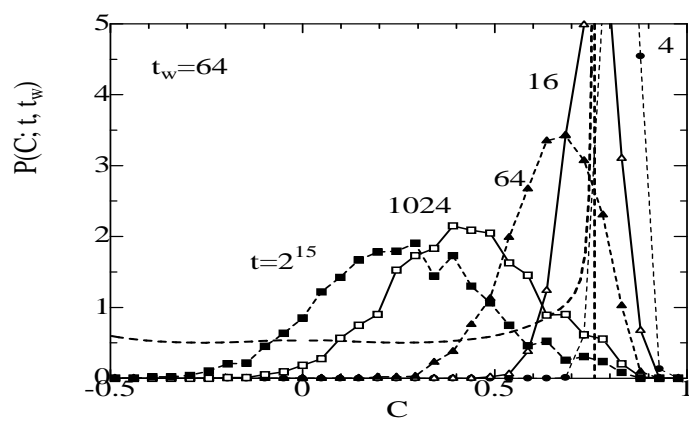


Fig. 10